


Article

Research on Solidification Layer Detection in Coal Transportation Process Based on Improved YOLOv8 Algorithm

Baokang Xiang , Ruihong Zhou *, Kaifeng Huang and Litong Dou

School of Mechanical and Electrical Engineering, Huainan Normal University, Huainan 232001, China; 18075307025@163.com (B.X.)

* Correspondence: zrh@hnnu.edu.cn

Abstract: Railway transportation is one of the main modes of long-distance coal transportation, and it inevitably causes environmental pollution during the transportation process. In order to improve the environment along the railway and increase the utilization rate of coal resources, this paper proposes a detection algorithm for the scattered coal solidification layer during transportation based on the YOLOv8 model and designs an intelligent recognition model suitable for coal solidification layer detection devices by combining fluorescence detection methods. Through experimental analysis, we found that the model meets the requirements of practical detection and can play a crucial role in environmental protection, with high practical application value.

Keywords: railway transportation; coal solidification layer; image processing; fluorescence detection



Citation: Xiang, B.; Zhou, R.; Huang, K.; Dou, L. Research on Solidification Layer Detection in Coal Transportation Process Based on Improved YOLOv8 Algorithm. *Processes* **2024**, *12*, 1211. <https://doi.org/10.3390/pr12061211>

Academic Editors: Stefania Tronci, Massimiliano Errico, Riccardo Bacci di Capaci, Ingmar Nopens, Elena Torfs and Michael Short

Received: 27 May 2024

Revised: 7 June 2024

Accepted: 12 June 2024

Published: 13 June 2024



Copyright: © 2024 by the authors. Licensee MDPI, Basel, Switzerland. This article is an open access article distributed under the terms and conditions of the Creative Commons Attribution (CC BY) license (<https://creativecommons.org/licenses/by/4.0/>).

1. Introduction

The distribution of coal resources in our country is uneven. In order for all regions to have sufficient coal resources, the key factor is transportation. As the main transportation tool for coal transportation, although railways have excellent characteristics such as low cost and large one-time transportation volume, they also have a significant impact on the environment [1]. Part of the actual rail transport of coal is transport of no real value. For example, during the transportation, due to the use of open car transportation and the frequent occurrence of external unstable factors, the coal powder in the carriage is easily blown away, resulting in a reduction in the quality of coal transportation in the railway system. In addition, the scattering of pulverized coal will also lead to a large amount of dust, which will bring serious harm to the surrounding environment and human health [2,3]. The authors of [4] analyzed the data of 50 stations in China from 2013 to 2016 and revealed the dynamic characteristics of invalid transport in the railway freight network by constructing the ineffective transport causal network (ITCN). Therefore, in order to improve the quality of coal transportation in the railway system, we must take into account the dynamic characteristics of the transportation process when conducting this study. Through its model, [5] showed us how to improve transportation efficiency and reduce potential transportation risks by optimizing parameters. Through careful parameter adjustment and system optimization, the model not only improves the transportation efficiency, but also significantly reduces the risk caused by the uncertainty in the transportation process, which provided a strong idea for this research paper.

The traditional coal dust detection method mainly relies on manual sampling, but the data obtained from manual sampling have a series of problems such as narrow coverage, a long detection cycle, and the inability to continuously detect [6]. Therefore, traditional detection methods cannot effectively detect coal dust, and the detection methods urgently need to be upgraded. It can be seen that in order to effectively control coal dust pollution and improve transportation quality, it is necessary to further improve the dust suppression quality during coal transportation. It is of great practical significance to study the

target detection algorithm in coal transportation and improve the accuracy of the target detection task.

Currently, there are two mainstream algorithms for object detection based on deep learning. The first type is a two-stage object detection algorithm represented by Faster R-CNN [7–9]. Another type is a single-stage object detection algorithm represented by the YOLO series [10–12]. Although the accuracy of two-stage algorithms is generally higher than that of single-stage algorithms, single-stage detection algorithms have high real-time performance and fast speed, and are highly favored by researchers. The YOLOv8 algorithm is the eighth generation of real-time object detection algorithms in the YOLO family. It provides real-time performance while maintaining high-precision detection and has many advantages such as high accuracy and fast speed. The YOLO algorithm has been widely used in various industries. Reference [13] proposes a small target detection method for unmanned aerial vehicle (UAV) aerial photography based on the improved YOLOv8 algorithm. The method uses an optimized gradient allocation strategy, introduces an attention module, and adopts a multi-scale fusion network, greatly improving the accuracy of target detection. Reference [14] used the lightweight YOLOv8 algorithm to detect tomatoes, using depthwise separable convolution technology instead of regular convolution. A dual-path attention module was designed, and a feature enhancement module was added to prevent effective feature loss and improve detection accuracy. Reference [15] studied the application of an improved YOLOv8 model in foreign object recognition and optimized and improved the model to ensure transmission security and efficiency. Reference [16] proposes a custom framework model based on image data, which introduces directional loss functions to achieve faster convergence and improve algorithm training and inference capabilities.

This article develops an improved coal solidification layer detection model based on YOLOv8 [17], which uses image-based data. Firstly, we changed the YOLOv8 activation function SiLu [18] to FReLU [19]. The replaced activation function can better express the target, significantly improving the training and inference capabilities of the detection algorithm. Secondly, due to the low pixel density of the coal solidification layer, it is easy to cause information loss. Therefore, the CBAM attention mechanism module is introduced into the network. The fusion of channel attention and spatial attention improves the accuracy of feature extraction and enhances the accuracy of classification recognition. Finally, fluorescence detection technology is introduced to specifically bind the fluorescent material with the coal solidification layer, emitting fluorescence and enhancing the detection of the coal solidification layer [20–23].

The remaining content of this article is as follows: Section 2 introduces the model of object detection and the improvement of the algorithms. Section 3 presents the relevant results of the experiments and analyzes them. Section 4 summarizes the research results.

2. Object Detection Model

Object detection is a hot topic in machine vision perception tasks. In the dust suppression monitoring system for railway coal transportation, the personnel and equipment can play a role in safety supervision and early warning. The overall architecture of the railway coal transportation target detection model proposed in this article is shown in Figure 1. The monitoring system mainly consists of a high-definition imaging unit, an intelligent recognition monitoring unit, a data transmission center, and a user terminal. It can monitor the detection effect of the coal solidification layer in real time and detect abnormal states in the detection process in a timely manner. The monitoring system detects the status of the solidified layer through high-definition imaging equipment, transmits video or image information to relevant departments, and is able to capture and recognize locomotive numbers. The high-definition imaging unit adopts a dual-redundant structure to improve the reliability of information during image acquisition. At present, China's 5G communication technology is developing rapidly, and long-distance transmission is achieved through 5G wireless communication technology.

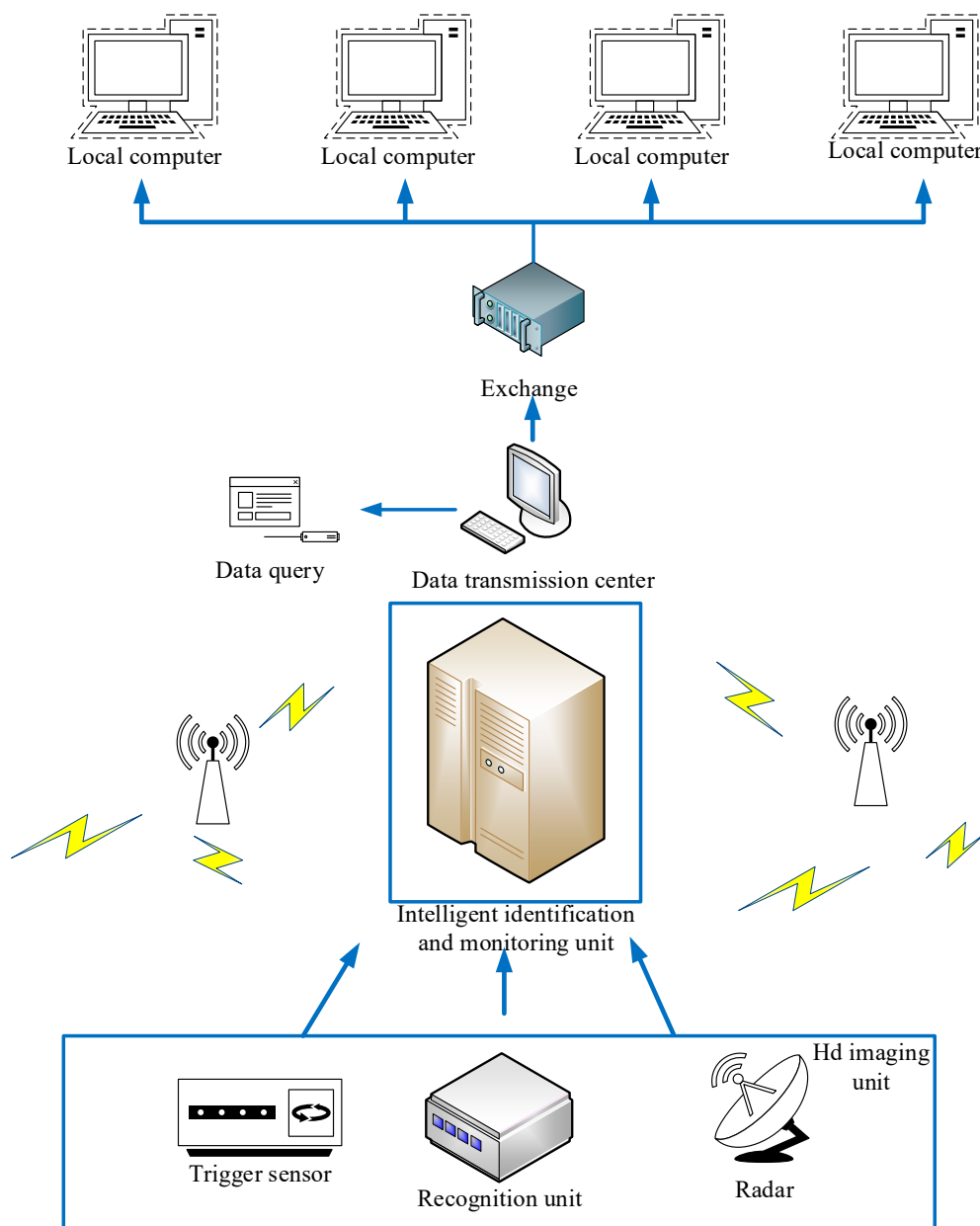


Figure 1. Monitoring system structure diagram.

2.1. YOLOv8 Object Detection Algorithm

The primary prerequisite for achieving abnormal state recognition during the detection process is to perform object detection on the collected images of the monitoring system. Compared to traditional image processing methods that manually select image features and set classification standards, the features obtained by machine vision methods have stronger generalization and robustness and are suitable for more complex scenes. The recognition of the solidified layer is based on image object detection, and the YOLOv8 network model is selected as the basic structure of the object detection algorithm [24]. Then, the network structure is fine-tuned according to the characteristics of complex images and large targets, ultimately achieving the intelligent recognition function of the solidified layer.

In the field of object detection, the YOLO series algorithms are often the preferred choice for a large number of object detection tasks in the industry due to their balance between accurate detection accuracy and efficient running speed. Since researchers proposed the object detection network YOLO in 2016, various versions have been derived, including improved and optimized versions from v1 to v8. The YOLOv8 algorithm has made new

improvements to the previous successful detection network models to further improve accuracy and real-time detection. One of the key features of YOLOv8 is extensibility, which is designed as a main framework that supports all YOLO versions, so we can easily compare their performance [25]. In addition, in the field of image detection, the algorithm contains other innovations. For example, the backbone network has selected C2f modules with richer gradient flow, and adjusts the number of channels for different scale models to form a neural network model with stronger feature representation ability. The detection head adopts the popular decoupling head structure of classification detection separation, which can clearly separate the classification head and detection head. A series of improvements have also been made in the calculation of loss functions and data augmentation, greatly improving the detection accuracy of the model.

The network structure of YOLOv8 to be improved in this paper is shown in Figure 2a, and the improved part is marked in a red box. YOLOv8 is divided into the backbone, neck, and head.

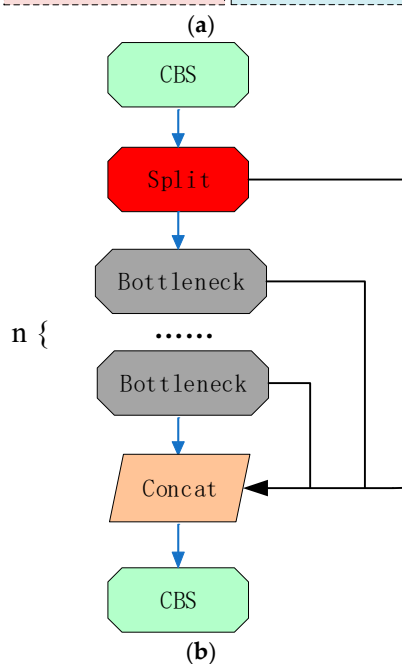
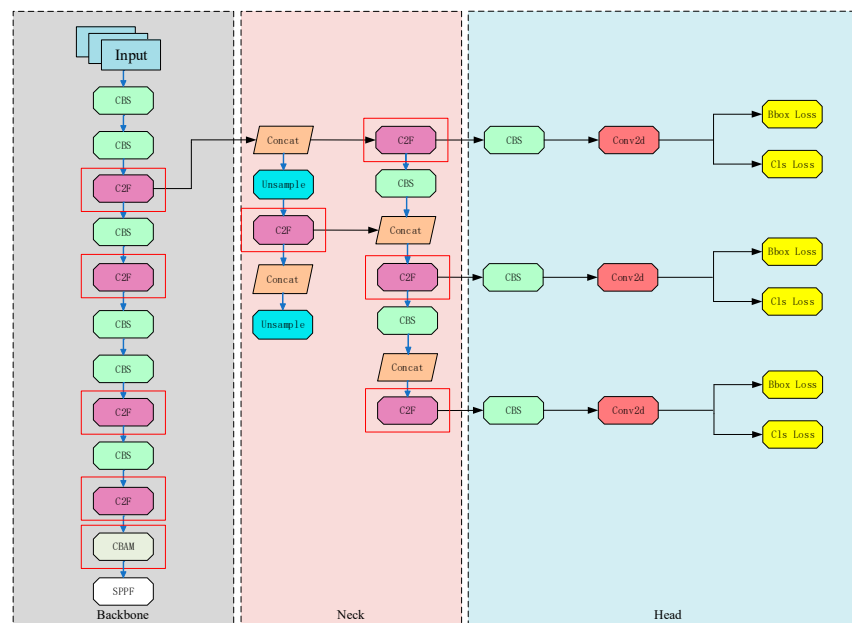


Figure 2. Cont.

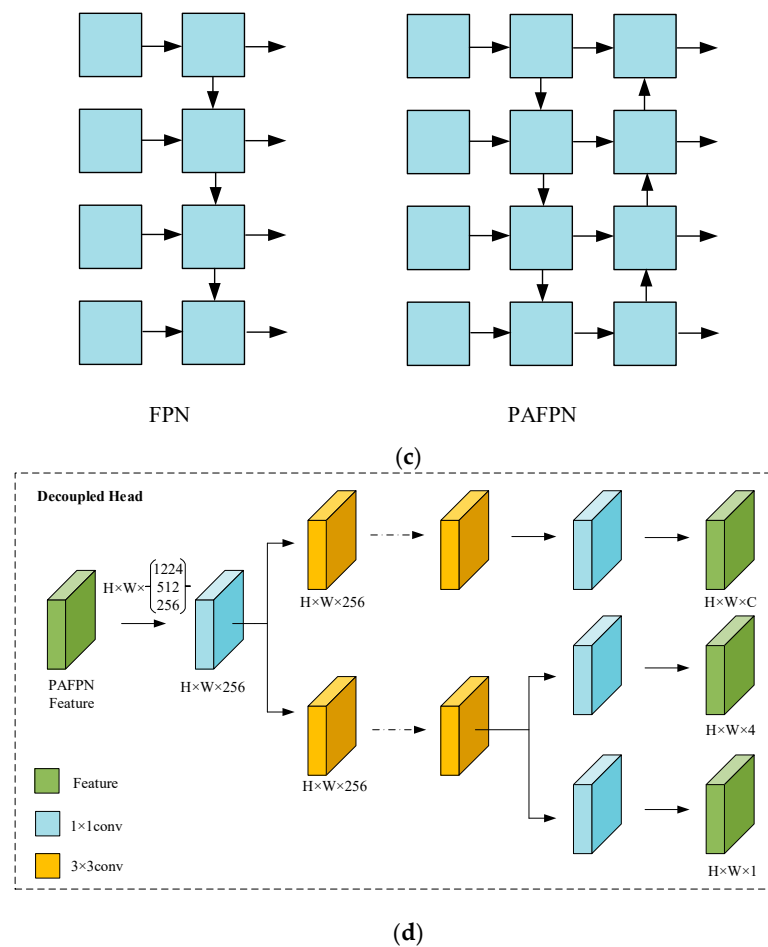


Figure 2. Improved YOLOv8 network structure diagram. The improved YOLOv8 network structure diagram is shown in (a,b) the C2f module structure diagram, (c) the FPN and PAFPN structure diagram, and (d) the decoupling head structure diagram.

- (1) The backbone uses the basic structure of CSPDarkNet53, and the image input is convolved at the first layer to obtain the output with the number of channels 64. After multiple convolution–batch normalization–SiLU activation and adding the C2f module, the three-scale spatial pyramid feature map is integrated by the fast spatial pyramid layer (SPPF). Enter to the neck section. In order to obtain more abundant gradient flow information, the backbone and neck replace the C3 module of YOLOv5 with the C2f module, which is composed of cross-layer convolution channels and several residual modules. Compared to the C3 module used by YOLO v5, C2f has more split modules and added skip links, which allows the C2f module of YOLOv8 to consider more information. Due to the deletion of a parallel convolution module, the parameter number of YOLO v5 is not much different from that of YOLO v5 under the condition of increasing skip layer links, and the real-time characteristics of the YOLO algorithm are maintained. The module structure diagram is shown in Figure 2b.
- (2) The neck part uses FPN+PAN architecture (PAFPN for short) to fuse multi-layer semantic information and make up for the underlying positioning features that are blurred after strengthening multi-layer convolution pooling. The early YOLO algorithm only used FPN, added top-down lines and horizontal connections, fused features at various levels, and built a feature pyramid with different scales and rich semantic information. In the top-down path, although FPN tries to recover the lost low-level features through horizontal connections, there is still a certain degree of information loss in the process. PAFPN is a further improved network architecture based on FPN. Through a more complex path aggregation strategy, PAFPN can com-

bine features from different levels more effectively, which helps to detect targets of different sizes more accurately, and at the same time can improve the problem of information loss in the information transmission process of FPN. The structure diagram of FPN and PAFPN is shown in Figure 2c.

- (3) The previous coupling head coupled multiple tasks to the same head to identify, and the model recognition accuracy was very low. Therefore, the decoupled head structure is chosen for the head part of this paper. Its core idea is to divide the complex model into multiple sub-models, each of which is responsible for performing a specific task or learning a specific representation. These sub-models are called “heads”. Each head can be trained independently, which reduces the complexity of the overall model, and then takes advantage of parallel computing to improve training efficiency. The network structure of the decoupling head is shown in Figure 2d. The feature graph obtained from the PAFPN structure is initially downsampled by 1×1 convolution, and the dimension of the feature channel is reduced to 256. Then, two parallel 3×3 convolution layer branches are introduced to complete the separation operation of classification and localization tasks. After the two parallel convolution layers, two parallel 1×1 convolution layers are connected to complete the localization and confidence detection tasks. After the above operations are completed, such a design reduces the dimension in feature processing and can simultaneously capture classification and position information in image features through parallel convolution branches, thus supporting model learning more effectively. At this point, the purpose of decoupling the head is basically realized.

2.2. Introduction of CBAM Attention Module

Due to the insufficient recognition features of the coal solidification layer, the attention module CBAM is introduced to improve the feature extraction ability of the model (the location where this mechanism is introduced is shown in Figure 2a) [26]. In order to focus the model on learning important features, the CBAM module ignores unimportant features and combines spatial and channel attention mechanisms to form a new structure. Because the CBAM module can adaptively adjust the feature extraction method, introducing the CBAM attention module can improve the performance of convolutional neural networks and overcome the shortcomings of YOLOv8 backbone networks in extracting important information features in fuzzy and dark environments, which have poor generalization ability, thereby improving the performance of the model [27].

When the input feature map of the model is $F \in R^{C \times H \times W}$ (F is the input feature map, R is the feature map with C channels, H height, and W width), first input the feature map into the channel attention module, output the corresponding attention map, then multiply the input feature map with the attention map, output it through the spatial attention module, perform the same operation, and finally obtain the output feature map. The CBAM network structure diagram is shown in Figure 3, and the process is as follows:

$$\begin{aligned} F' &= M_c(F) \otimes F \\ F'' &= M_s(F') \otimes F' \end{aligned} \quad (1)$$

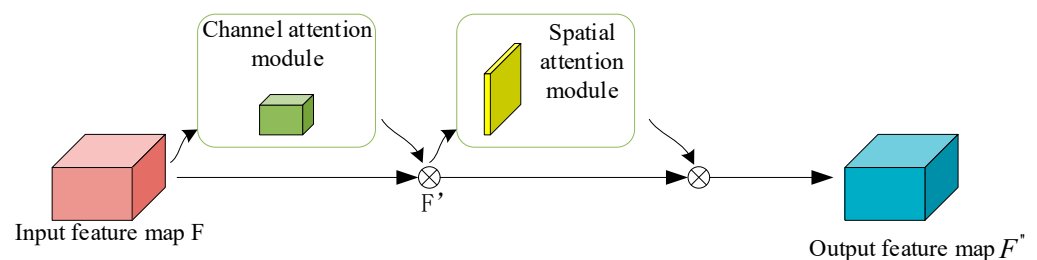


Figure 3. CBAM Network Structure.

\otimes is element-level multiplication, F'' is the final output feature, $M_c \in R^{1 \times 1 \times C}$ is a one-dimensional channel attention module diagram, and $M_s \in R^{W \times H \times 1}$ is a two-dimensional channel attention module diagram. The CBAM attention submodule diagram is shown in Figure 4.

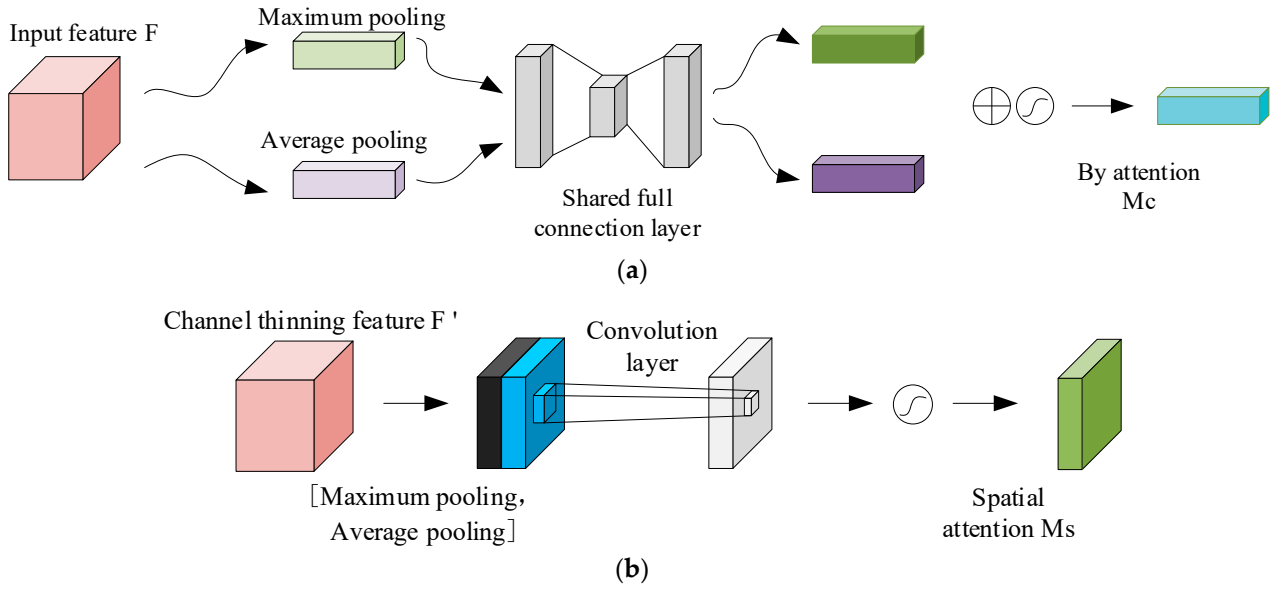


Figure 4. Structure diagram of CBAM submodule. (a) Structure diagram of channel attention module; (b) Structure diagram of spatial attention module.

In the channel attention module, the input feature map F is first subjected to width- and height-based average pooling and maximum pooling operations to obtain two different spatial descriptors: F_{avg}^c and F_{max}^c , which are average pooling and maximum pooling features, respectively. These two descriptors are then transmitted to a shared fully connected layer composed of multi-layer perceptrons (MLPs) and a hidden layer. The obtained output elements are added one by one and the sigmoid activation function is used to obtain the channel attention feature $M_c(F)$. The expression is as follows:

$$M_c(F) = \sigma(MLP(avgPool(F)) + MLP(maxPool(F))) = \sigma(W_1(W_0(F_{avg}^c)) + W_1(W_0(F_{max}^c))) \quad (2)$$

σ is the sigmoid activation function, and $W_0 \in R^{(C/r) \times C}$, $W_1 \in R^{C \times (C/r)}$, and r are dimensionality reduction factors.

In the spatial attention module, the input feature graph is first obtained based on channel average pooling and maximum pooling operations, and the feature graph is combined to obtain the feature graph with channel number 2. Then, the channel number is reduced to 1 through the 7×7 convolution layer, and finally the spatial attention feature is obtained through the sigmoid activation function, the expression is as follows:

$$M_s(F) = \sigma(f^{7 \times 7}([avgPool(F); maxPool(F)])) = \sigma(f^{7 \times 7}([F_{avg}^S; F_{max}^S])) \quad (3)$$

σ is the sigmoid activation function, and $f^{7 \times 7}$ is a convolution with a kernel of 7×7 .

The CBAM attention mechanism combines the channel attention mechanism and spatial attention mechanism to improve the expression ability of feature maps at different levels. The CBAM attention mechanism utilizes channel and spatial attention mechanisms to selectively enhance the network's attention to key features, reduce irrelevant information interference, improve the model's performance in tasks such as object detection and image recognition, and enhance the model's generalization ability and robustness. We introduced the CBAM attention module into the blue section shown in Figure 5.

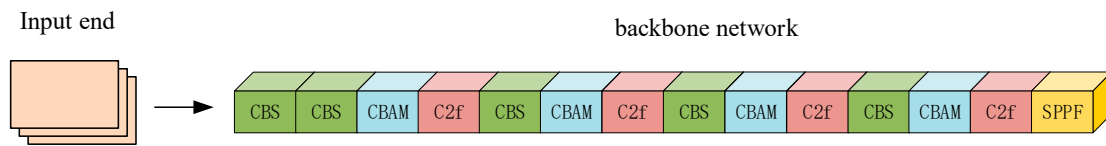


Figure 5. CBAM backbone network structure diagram.

2.3. Replacing Activation Functions

In order to improve the expression ability of neural networks for models, solve problems that linear models cannot solve, and enhance the expression ability of convolutional neural networks, we replaced the SiLU function (Sigmoid Weighted Linear Unit) with the FReLU activation function [28,29]. FReLU is known as funnel activation in the field of image recognition, which extends ReLU and PReLU to 2D activation by adding funnel conditions to improve machine vision tasks. The expression for this process is as follows:

$$F = \max(x, T(x)) \quad (4)$$

Due to the high background interference and detection difficulty in the recognition task of the monitoring system, a more powerful feature extraction network is needed in the feature fusion part. NAS-FPN uses NAS (Neural Architecture Search) technology to optimize the architecture of FPNs (Feature Pyramid Networks). This method uses a search instead of manually planning feature fusion between different scales, making it excellent in feature fusion and not significantly affecting computational speed [30]. The activation characteristics of the FReLU activation function are shown in Figure 6.

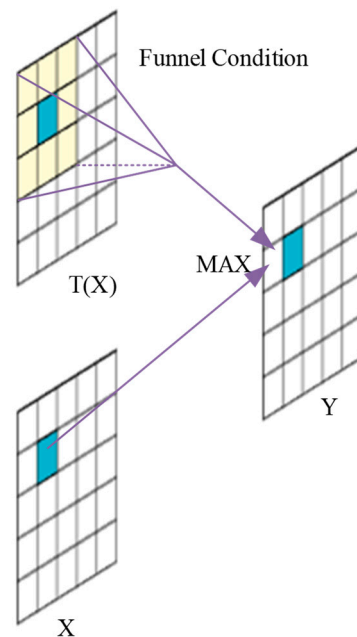


Figure 6. Characteristics of FReLU activation function.

From this, it can be seen that using the FReLU activation function has better context capture ability, has better expression of fuzzy and small target objects, and enables the system to have a wider activation domain, which plays a crucial role in the construction of the system.

2.4. Introduction of CQDs-MIPs Fluorescence Detection Technology

In this study, the detection process of CQDs-MIPs fluorescence detection technology includes [31] the recognition and capture of target substances and the recognition output of fluorescence signals. The recognition and capture of target substances are achieved through

molecular imprinting technology: molecularly imprinted polymers (MIPs) have specificity and can bind with the target substance to form specific recognition sites (the white star on the left is the recognition site). When the target substance exists, it interacts with MIPs and is captured at the recognition site. The recognition output of fluorescence signals is achieved through CQDs fluorescence detection technology: after the target substance is combined with CQDs-MIPs composite materials, the fluorescence signal of CQDs changes, which is used as an indicator of the presence of the target substance. The intensity changes of the fluorescence signals are measured and recorded to determine the presence of the target substance. Figure 7 reveals the process of CQDs-MIPs fluorescence detection technology.

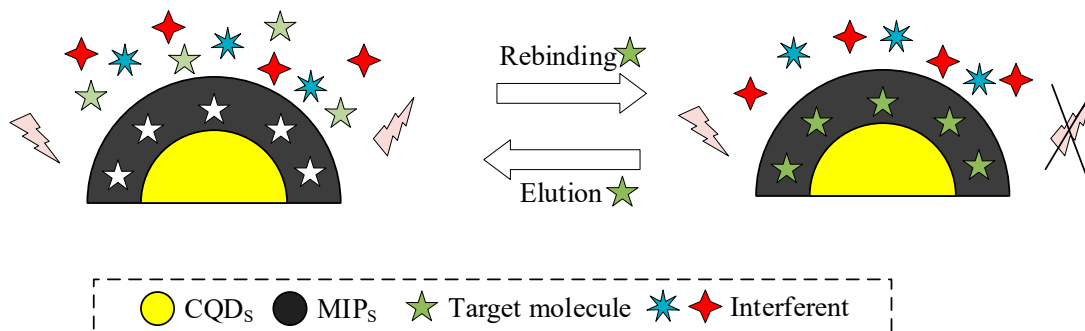


Figure 7. Schematic diagram of CQDs-MIPs fluorescence detection technology.

The fluorescence intelligent recognition monitoring device is set on the fluorescence channel light path of the multi-channel fluorescence microscope, allowing the device to continuously capture the fluorescence emitted by the multi-channel fluorescence microscope and convert the captured external light information into a signal that can be recognized by the computer system through a microprocessor. Then, the converted signal is sent to the computer system, allowing the computer system to automatically configure the corresponding information based on the signal.

3. Experimental Analysis

3.1. Experimental Environment and Data

The specific experimental environment is shown in Table 1.

Table 1. Experimental Environment.

Configuration Name	Version Parameter
Operating system	Windows 11
CPU	AMD Ryzen 5 5600H
GPU	NVIDIA GeForce RTX 3050
Store	8 GB
Algorithm framework	PyTorch 1.11.0

The sample data of this experiment were collected through real-time dust suppression monitoring video, which included image data from different environments, angles, and models. The Labelling script tool was used to annotate the image data. In order to enhance the generalization ability of the model, 6000 images were randomly selected as the training set and 1500 images as the testing set. The hyperparameters of the model were set based on prior knowledge, and the total epoch of the model was set to 300. To prevent overfitting, the learning rate of the first epoch was set to 0.01, and the learning rate of the last 100 epochs was set to 0.001. Some examples of the datasets are shown in Figure 8.



Figure 8. Monitoring Image Dataset.

3.2. Recognition Effect of the Model

In this study, the basic YOLOv8 network model, the YOLOv8_C network model introducing the attention module, the YOLOv8_F network model replacing the activation function, and the CQDS-MIPs fluorescence detection technology combined with the YOLOv8_M network model were compared and analyzed. Figure 9 shows the convergence process of the Loss curve of the verification set. It is not difficult to see that after about 50 iterations, the loss of YOLOv8 finally stabilized at about 0.6. The loss of YOLOv8_C and YOLOv8_F network models with attention module and replacement activation function is stable at 0.5 and 0.3. The final loss of YOLOv8_M network model combined with fluorescence detection technology is reduced to about 0.23, which is generally lower than the previous three YOLO algorithms.

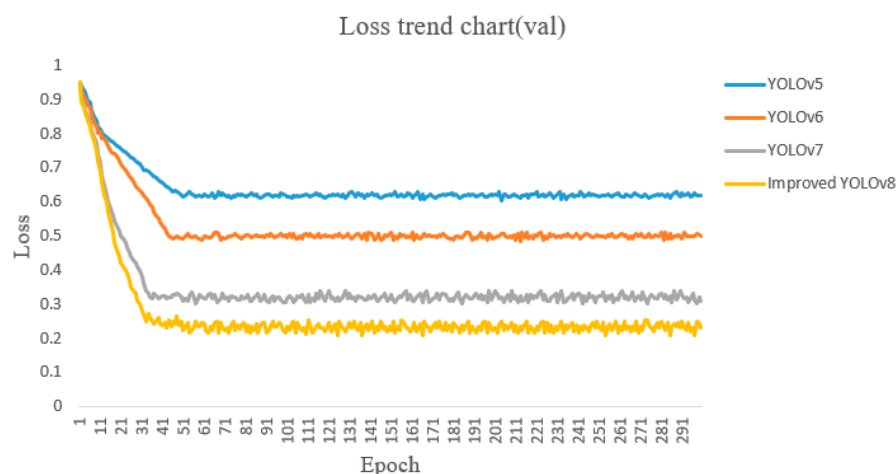


Figure 9. Comparison of loss convergence curves.

3.3. Analysis of Model Recognition Effect

After the above model training is completed, we usually use accuracy (P), recall rate (R), average accuracy (mAP), size of storage space occupied (MB), and frame rate per second (FPS) as indicators to evaluate algorithm performance. The calculation formula for several performance indicators is as follows:

$$P = \frac{TP}{TP + FP} \tag{5}$$

$$R = \frac{TP}{TP + FN} \tag{6}$$

$$AP = \int_0^1 P(R) dR \tag{7}$$

Degree refers to the proportion of samples that are truly positive in the model among all samples predicted as positive by the model. In the above formula, True Positions (*TPs*) are the number of samples correctly predicted as positive categories by the model, and False Positions (*FPs*) are the number of samples incorrectly predicted as positive categories by the model. The higher the *p*-value, the lower the false positive rate. The recall rate refers to the proportion of samples that the model successfully predicts as positive categories among all samples that are truly positive. Among them, False Negatives (*FNs*) are the number of samples that the model incorrectly predicts as negative categories. The higher the *R*-value, the lower the false negative rate. Table 2 shows the comparison of indicators for different models.

Table 2. Comparison of Model Indicators.

Model	<i>P</i> %	<i>R</i> %	mAP@0.5/%	Weight/MB	<i>FPs</i>
YOLO_v8	91.89	87.63	84.6	7.2	34.3
YOLOv8_C	92.46	89.52	88.7	7.4	19.8
YOLOv8_F	94.38	92.87	86.9	7.6	23.5
YOLOv8_M	97.12	95.38	90.8	7.2	32.6

From the above table, it can be seen that the improved YOLOv8 has better performance, with a *p*-value of 97.12%, an *R*-value of 96.48%, and an average accuracy of 97.38%. These indicators prove the effectiveness of YOLOv8_M model combined with fluorescence detection technology. It can also be seen that the detection speed of the original YOLOv8 is slightly better than the improved algorithm model, but the difference in detection accuracy compared to the improved model is too great, which can lead to too many false detections and missed detections for the needs of actual industrial scene detection.

Overall, the algorithm proposed in this article has advantages such as fewer network parameters, low computational complexity, good algorithm robustness, high detection accuracy, and fast processing speed. It can effectively detect dust in the coal solidification layer, thereby reducing dust emissions during railway coal transportation and achieving dust suppression.

3.4. Ablation Experiment

In order to further verify the effectiveness of each improved module of the algorithm proposed in this article, ablation experiments were conducted on the baseline model. The ablation experiments were gradually carried out by replacing the activation function FReLU, introducing the CBAM attention module, and combining CQDs-MIPs fluorescence detection technology. This study used the same equipment and dataset for the experiments, and the experimental results are shown in Table 3, where “√” indicates the introduction of this method.

Table 3. Comparison of Objective Indicators in Ablation Experiments.

Model	YOLOv8	FReLU	CBAM	CQDs-MIPs	<i>P</i> %	<i>R</i> %	<i>FPs</i>
A	√				90.89	87.63	34.3
B	√	√			91.37	88.59	36.8
C	√		√		92.68	89.64	35.4
D	√			√	92.43	89.91	34.3
E	√	√	√		96.74	95.82	38.5
F	√	√		√	93.62	90.75	42.5
G	√		√	√	94.98	93.72	41.1
H	√	√	√	√	95.85	94.27	44

From Table 3 and Figure 10, it can be seen that in the improved model based on the original YOLOv8 algorithm, both *P* and *R* have been improved to varying degrees. By only

introducing CQDs-MIPs fluorescence detection technology, the model architecture remains unchanged, so *FPS* is not affected. The E model *P* and *R* improved by 5.85% and 8.19%, respectively, making them the most successful ablation experimental group. However, their computational complexity increased accordingly, and the *FPS* was lower than the final H model, resulting in a slower recognition speed of the model. By combining FReLU, CBAM, and CQDs-MIPs, the improved model achieved *P* and *R* of 95.85% and 94.27%, respectively, with a recognition speed of 44 frames per second. Compared to the original model, *P* and *R* increased by 4.96% and 6.64%, respectively, and *FPS* increased by 128.28%, significantly improving the recognition speed and accuracy of the original model and further proving the effectiveness of the improved model.

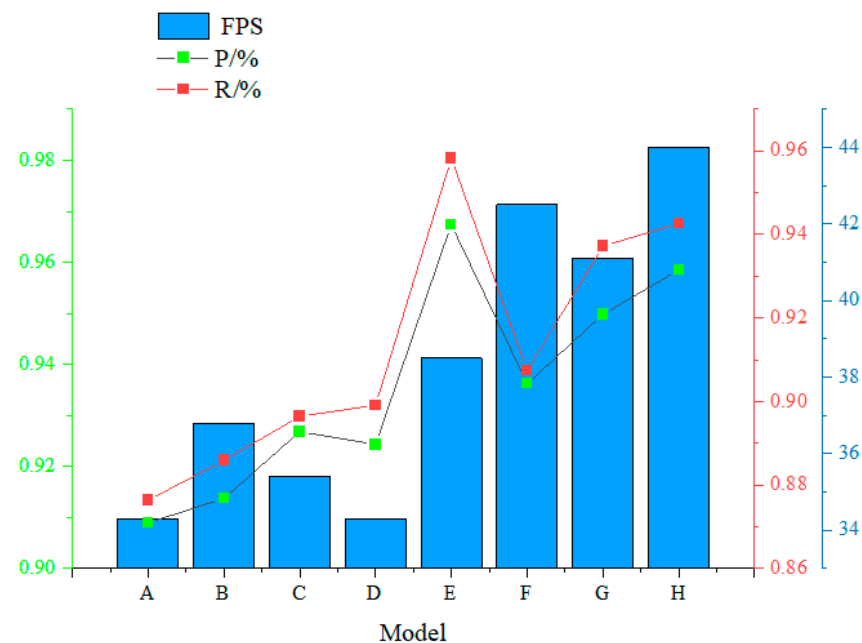


Figure 10. Results of ablation experiment.

4. Conclusions

Aiming at the problem of coal dust in the process of railway transportation, this paper innovatively proposes an improved YOLOv8 model, which improves the detection accuracy of the coal solidified layer. After a series of experiments, the practicality of the improved model was proven. The experimental results are as follows:

- (1) Firstly, introducing the CBAM attention module into the YOLOv8 model can enhance its feature extraction and antiredundant feature capabilities. Compared with the original YOLOv8 model, the improved model increased accuracy (*P*) and recall (*R*) by 1.79% and 2.01%, respectively, indicating that the attention mechanism plays a crucial role in improving the accuracy of object detection tasks.
- (2) Replacing FReLU as the activation function effectively maps the activated neuron features by retaining basic features and eliminating redundancy, thereby enhancing the expressive power of convolutional neural networks and improving the frame rate (*FPS*) of the model to a certain extent. We believe that this can improve real-time performance in practical applications.
- (3) The introduction of CQDs-MIPs fluorescence detection technology, with its high sensitivity and resolution, can quickly identify whether the coal solidification layer is damaged and has great development space in practical application scenarios.
- (4) By introducing CBAM, replacing activation functions, and introducing fluorescence detection technology, the accuracy and recognition speed of the improved YOLOv8 model have been significantly improved. In the experiment, the accuracy (*P*) of the model was 95.85%, the recall (*R*) was 94.27%, and the recognition speed was

44 frames per second. This indicates that the model has strong practicality in object detection tasks.

Author Contributions: Conceptualization, B.X. and R.Z.; methodology, B.X.; software, R.Z.; validation, L.D. and K.H.; formal analysis, B.X.; investigation, K.H. and L.D.; resources, R.Z.; data curation, K.H.; writing—original draft preparation, B.X.; writing—review and editing, B.X.; visualization, R.Z.; supervision, K.H.; project administration, K.H.; funding acquisition, K.H. All authors have read and agreed to the published version of the manuscript.

Funding: This research was funded by the Open Fund of State Key Laboratory in 2022 “Research on Intelligent Diagnosis Technology of Safety Monitoring Sensor Based on Deep Learning Algorithm” (grant number SKLMRDPC21KF23), Natural Science Research Key Project of Anhui Provincial Department of Education “Research on impact dynamics characteristics and instability modes of deep coal-rock combinations” (grant number 2022AH051573), and Huainan Normal University 2022 Campus level Natural Science Research Project “Research on Large scale Multi antenna Non stationary Characteristics Communication System” (grant number 2022XJYB035).

Data Availability Statement: The data that support the findings of this study are available from the corresponding author upon reasonable request.

Conflicts of Interest: The authors declare no conflicts of interest.

References

1. Wang, Y.J.; Sun, Q.Q.; Wu, J.J. Research on the low carbon development path of China’s coal industry under carbon peaking & carbon neutral target: Based on the RCPs-SSPs framework. *Resour. Policy* **2023**, *86*, 104091.
2. Lu, M.; Yan, P.; Li, T.C. Research on dust control countermeasures based on Zhangshuanglou Coal Mine Industrial square. *Energy Technol. Manag.* **2023**, *48*, 197–198.
3. Trechera, P.; Moreno, T. Comprehensive evaluation of potential coal mine dust emissions in an open-pit coal mine in Northwest China. *Int. J. Coal Geol.* **2021**, *15*, 103677. [[CrossRef](#)]
4. Khachatryan, N.K.; Akopov, A.S. Model for organizing cargo transportation with an initial station of departure and a final station of cargo distribution. *Бизнес-Информатика* **2017**, *1*, 25–35. [[CrossRef](#)]
5. Yuan, Y.; Jiang, X.; Yuanxun, L. An ineffective transport-focused, causality-based approach to station-to-station railway freight network design. *IEEE Access* **2020**, *8*, 143891–143901. [[CrossRef](#)]
6. Qiu, J.; Su, Z.T.; Wu, D.H. Study on comprehensive evaluation of coal mine dust health risk. *China Min. Mag.* **2021**, *30*, 155–162.
7. Cao, C.; Wang, B.; Zhang, W. An improved faster R-CNN for small object detection. *IEEE Access* **2019**, *7*, 106838–106846. [[CrossRef](#)]
8. Cai, Z.; Vasconcelos, N. Cascade R-CNN: High quality object detection and instance segmentation. *IEEE Trans. Pattern Anal. Mach. Intell.* **2019**, *43*, 1483–1498. [[CrossRef](#)] [[PubMed](#)]
9. Richard, B.; Karen, S.; Julio, C. A deep learning system for collotelinite segmentation and coal reflectance determination. *Int. J. Coal Geol.* **2022**, *263*, 104111.
10. Li, D.Y.; Wang, G.F.; Guo, Y.C. An identification and positioning method for coal gangue based on lightweight mixed domain attention. *Int. J. Coal Prep. Util.* **2023**, *43*, 1542–1560. [[CrossRef](#)]
11. Li, M.; He, X.L.; Yuan, X.Y. Multiple factors influence coal and gangue image recognition method and experimental research based on deep learning. *Int. J. Coal Prep. Util.* **2023**, *43*, 1411–1427. [[CrossRef](#)]
12. Ahmad, T.; Ma, Y.; Yahya, M.; Ahmad, B.; Nazir, S.; Haq, A.U. Object detection through modified YOLO neural network. *Sci. Program.* **2020**, *2020*, 1–10. [[CrossRef](#)]
13. Wang, G.; Chen, Y.F.; An, P. UAV-YOLOv8: A Small-Object-Detection Model Based on Improved YOLOv8 for UAV Aerial Photography Scenarios. *Sensors* **2023**, *23*, 7190. [[CrossRef](#)] [[PubMed](#)]
14. Yang, G.L.; Wang, J.X.; Nie, Z.L. A Lightweight YOLOv8 Tomato Detection Algorithm Combining Feature Enhancement and Attention. *Agronomy* **2023**, *13*, 1824. [[CrossRef](#)]
15. Luo, B.X.; Kou, Z.M.; Han, C. A “Hardware-Friendly” Foreign Object Identification Method for Belt Conveyors Based on Improved YOLOv8. *Appl. Sci.* **2023**, *13*, 11464. [[CrossRef](#)]
16. Xue, Q.L.; Lin, H.F.; Wang, F. FCDM: An Improved Forest Fire Classification and Detection Model Based on YOLOv5. *Forests* **2022**, *13*, 2129. [[CrossRef](#)]
17. YOLOv8-TensorRT. Available online: <https://github.com/triple-Mu/YOLOv8-TensorRT> (accessed on 24 March 2024).
18. Gou, X.T.; Tao, M.J.; Li, X. Real-time human pose estimation network based on wide receiving domain. *Comput. Eng. Des.* **2023**, *44*, 247–254.
19. Ma, N.N.; Zhang, X.Y.; Sun, J. Funnel Activation for Visual Recognition. *Comput. Vis.-ECCV 2020* **2020**, *12356*, 351–368.
20. Guo, X.; Zhou, L.; Liu, X. Fluorescence detection platform of metal-organic frameworks for biomarkers. *Colloids Surf. B Biointerfaces* **2023**, *229*, 113455. [[CrossRef](#)]

21. He, H.; Sun, D.W.; Wu, Z. On-off-on fluorescent nanosensing: Materials, detection strategies and recent food applications. *Trends Food Sci. Technol.* **2022**, *119*, 243–256. [[CrossRef](#)]
22. Sargazi, S.; Fatima, I.; Kiani, M.H. Fluorescent-based nanosensors for selective detection of a wide range of biological macromolecules: A comprehensive review. *Int. J. Biol. Macromol.* **2022**, *206*, 115–147. [[CrossRef](#)] [[PubMed](#)]
23. Xiong, H.; Qian, N.; Miao, Y. Super-resolution vibrational microscopy by stimulated Raman excited fluorescence. *Light Sci. Appl.* **2021**, *10*, 87. [[CrossRef](#)] [[PubMed](#)]
24. Zhang, M.; Zhang, Y.; Zhou, M. Application of Lightweight Convolutional Neural Network for Damage Detection of Conveyor Belt. *Appl. Sci.* **2021**, *11*, 7282. [[CrossRef](#)]
25. Lou, H.; Duan, X.; Guo, J. DC-YOLOv8: Small-Size Object Detection Algorithm Based on Camera Sensor. *Electronics* **2023**, *12*, 2323. [[CrossRef](#)]
26. Huang, K.F.; Li, S.Y.; Cai, F. Detection of Large Foreign Objects on Coal Mine Belt Conveyor Based on Improved. *Processes* **2023**, *11*, 2469. [[CrossRef](#)]
27. Fu, H.; Song, G.; Wang, Y. Improved YOLOv4 marine target detection combined with CBAM. *Symmetry* **2021**, *13*, 623. [[CrossRef](#)]
28. Varshney, M.; Singh, P. Optimizing nonlinear activation function for convolutional neural networks. *Signal Image Video Process.* **2021**, *15*, 1323–1330. [[CrossRef](#)]
29. Xiang, X.; Kong, X.; Qiu, Y. Self-supervised monocular trained depth estimation using triplet attention and funnel activation. *Neural Process. Lett.* **2021**, *53*, 4489–4506. [[CrossRef](#)]
30. Li, J.; Huang, Z.; Wang, Y. Sea and Land Segmentation of Optical Remote Sensing Images Based on U-Net Optimization. *Remote Sens.* **2022**, *14*, 4163. [[CrossRef](#)]
31. Xu, Q.; Xiao, F.; Xu, H. Fluorescent detection of emerging virus based on nanoparticles: From synthesis to application. *TrAC Trends Anal. Chem.* **2023**, *161*, 116999. [[CrossRef](#)]

Disclaimer/Publisher's Note: The statements, opinions and data contained in all publications are solely those of the individual author(s) and contributor(s) and not of MDPI and/or the editor(s). MDPI and/or the editor(s) disclaim responsibility for any injury to people or property resulting from any ideas, methods, instructions or products referred to in the content.